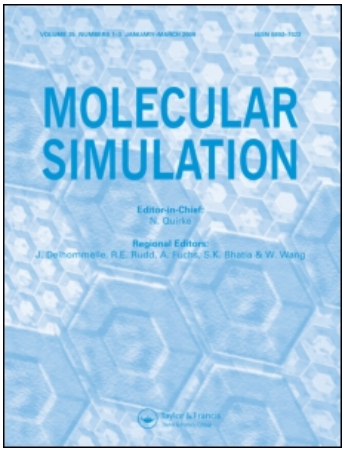

Molecular Simulation
Publication details, including instructions for authors and subscription information:
http://www.informaworld.com/smpp/title~content=t713644482

Influence of Simulation Details on Thermodynamic and Transport Properties in Molecular Dynamics of Fully Flexible Molecular Models

Peter A. Gordon[a]
[a] Corporate Strategic Research, ExxonMobil Research & Engineering, Annandale, NJ, USA

Online publication date: 26 October 2010

To cite this Article Gordon, Peter A.(2003) 'Influence of Simulation Details on Thermodynamic and Transport Properties in Molecular Dynamics of Fully Flexible Molecular Models', Molecular Simulation, 29: 8, 479 — 487
To link to this Article: DOI: 10.1080/0892702031000106669
URL: http://dx.doi.org/10.1080/0892702031000106669

Molecular Simulation, Vol. 29 (8), August 2003, pp. 479–487

Influence of Simulation Details on Thermodynamic and Transport Properties in Molecular Dynamics of Fully Flexible Molecular Models

PETER A. GORDON

Corporate Strategic Research, ExxonMobil Research & Engineering, Annandale, NJ 08801, USA

(Received November 2002; In final form February 2003)

In this work, we examine the impact of details of molecular dynamics simulation and data analysis protocols on resulting thermodynamic and transport properties of interest in the study of lubricant components. Of particular importance is understanding how viscosity computed from the fluctuation–dissipation formalism is influenced by simulation details, including the differences obtained between employing an atomic vs. molecular formalism to describe the stress tensor, the impact of the size of timestep, and the type of integration scheme employed. Understanding how these simulation details affect the computed properties of interest helps us to establish simulation protocols for examining transport properties of low molecular weight isomers, where we hope to resolve differences in transport properties as a function of fine structural features of the molecules.

Keywords: Viscosity; Equilibrium molecular dynamics; Lubricants; Thermodynamic and transport properties

INTRODUCTION

With the continuing improvements and availability of low cost, high performance cluster computing options, equilibrium molecular dynamics (EMD) simulation has found increasing application in the prediction of thermodynamic and transport properties of complex fluids relevant to lubricants. When EMD is applied to molecular liquids, however, the resulting properties can be quite sensitive to details concerning how the simulations are conducted, details which often are glossed over in the literature.

A number of workers have considered the effect of integration details, including size of timestep, on simulation results. A reasonable summary of such studies is that the impact of round-off and truncation errors associated with approximate integration schemes and limited machine precision generally has little effect on time averages for thermodynamic properties. Time-dependent properties such as autocorrelation functions and resulting transport coefficients may be more adversely affected, particularly when the relevant timescales over which such functions decay are long [1–3]. Complicating the situation, conclusions reached from studies on one type of system may not be directly applicable to another.

Understanding the influence of simulation details on time-dependent properties is complex because it is difficult to independently study the multiple sources of potential bias that could influence time correlations. It has been established that phonon corruption from finite-sized systems, artificial correlations due to structure imposed by periodically bounded systems, and propagation of errors from inaccuracies of the integration of the equations of motion all can influence time correlation functions. If we attempt to assess the influence of system size on a transport coefficient by performing simulations on a series of larger systems by increasing system size, the time scale at which phonon corruption may (or may not) influence time dependent properties changes. In addition, this phenomena would influence the system variables (positions and momenta) burdened with a different characteristic degree of round-off and truncation error because the timescale for the propagation of these effects has increased.

The purpose of this note is to examine the impact of details of simulation and data analysis protocols on resulting thermodynamic and transport properties of

ISSN 0892-7022 print/ISSN 1029-0435 online © 2003 Taylor & Francis Ltd
DOI: 10.1080/0892702031000106669

interest in the study of lubricant components. Of particular importance is understanding the differences between employing an atomic vs. molecular formalism to describe the stress tensor, the impact of the size of timestep and the type of integration scheme employed. This effort was deemed necessary in support of the analysis of transport properties of isomers of low molecular weight, where one hopes to resolve fairly small differences in transport properties as a function of similar types of molecular structure [4]. Care must be taken to ensure that transport properties are computed while removing (or understanding the effects of) any potential bias imparted to the results stemming from simulation details.

MODELS AND METHODS

Two systems were chosen for study in this work, 120 molecules of liquid *n*-octane at $T = 293\,\mathrm{K}$ and $\rho = 0.7126\,\mathrm{g/cm^3}$ and *n*-dodecane at $T = 373\,\mathrm{K}$ and $\rho = 0.7034\,\mathrm{g/cm^3}$. The paraffin molecule was modeled using the TRAPPE-United Atom potential parameterized by Martin and Siepmann [5] In this representation, hydrogen atoms are lumped with their bonded carbon neighbors to form an effective interaction site. This description significantly reduces the computational requirements necessary to compute interactions among neighboring molecules. The resulting united atom group interacts with a Lennard–Jones potential with all sites on neighboring molecules and with intramolecular sites separated by 3 or more bonds. Lorentz–Berthelot mixing rules are applied to cross interactions of Lennard–Jones parameters. Intramolecular degrees of freedom are constrained by interaction potentials governing bond lengths, bond angle bending, dihedral rotation about bonds, and umbrella inversion of single branch points. With the exception of dihedral rotation, a harmonic potential is used to govern the geometry. The dihedral rotation is given by the OPLS potential [6]. Non-bonded interactions were truncated at 10 Å. Many variables that follow are reported as standard non-dimensionalized quantities with $\sigma_{CH3} = 3.75\,\text{Å}$, $\varepsilon_{CH3} = 0.1946\,\mathrm{kcal/mol}$, and $m_{CH3} = 15.035\,\mathrm{g/mol}$.

All molecular dynamics simulations were performed using LAMMPS99, a parallelized molecular dynamics engine suitable for atomic and molecular systems [7], and modifications therein. The equations of motion were integrated either with a velocity Verlet algorithm, or with a multiple time step reversible extended system propagator algorithm (MTS-RESPA) [8,9]. The latter approach takes advantage of the fact that motion of different types of interactions evolve on differing timescales. The scheme supported in LAMMPS99 allows us to define several separate timesteps: δt_{bond} for fast varying harmonic bonds, $\delta t_{3-4\,\mathrm{intra}}$ for 3 and 4 body intramolecular interactions, and δt_{LJ} for slower varying short range Lennard–Jones forces.

The influence of the details concerning integration of the equations of motion was examined for both thermodynamic and transport coefficients computed through Green–Kubo relationships. All simulations were performed in the microcanonical (NVE) ensemble starting from the same initial equilibrated configuration of the liquid *n*-octane at the state point mentioned above. Details of the integrator scheme, size of $\delta t_{\mathrm{outer}}$, the outermost timestep, and breakdown of multiple timestep scheme (if employed) for runs discussed below are summarized in Table I. We treat the influence of the integration scheme on

TABLE I Integration timestep parameters in runs of *n*-octane reported in this work, along with atomic and molecular pressures computed over 2–3 ns trajectories.

Run	$\delta t_{(outer)}$ *(fs)*	$\delta t_{(bond)}$ *(fs)*	$\delta t_{(3-4\,intra)}$ *(fs)*	$\delta t_{(LJ)}$ *(fs)*	$\langle P^*_{at} \rangle$	σ	$< P^*_{mol} >$	σ
1	1.0				1.59	0.07	1.58	0.11
2	2.0				1.56	0.10	1.65	0.07
3	3.0		Verlet integrator employed		1.45	0.13	1.66	0.13
4	4.0				1.24	0.18	1.64	0.15
5	5.0				1.23	0.16	1.84	0.09
6	2.0	0.5	2.0	2.0	1.55	0.15	1.60	0.08
7	2.0	0.5	1.0	2.0	1.54	0.14	1.62	0.14
8	2.0	0.5	0.5	2.0	1.54	0.11	1.57	0.07
9	4.0	1.0	4.0	4.0	1.28	0.10	1.61	0.09
10	4.0	1.0	2.0	4.0	1.33	0.14	1.53	0.12
11	4.0	1.0	1.0	4.0	1.46	0.14	1.54	0.09
12	8.0	1.0	8.0	8.0	1.35	0.63	2.79	0.74
13	8.0	1.0	4.0	8.0	0.83	0.08	1.63	0.07
14	8.0	1.0	2.0	8.0	0.97	0.11	1.61	0.09
15	8.0	1.0	1.0	8.0	0.97	0.08	1.60	0.06
16	6.0	1.0	3.0	6.0	1.17	0.05	1.60	0.05
17	6.0	1.0	2.0	6.0	1.23	0.06	1.61	0.06
18	6.0	1.0	1.0	6.0	1.24	0.06	1.56	0.07
19	2.0	1.0	2.0	2.0	1.55	0.05	1.58	0.04

each property in turn by referring to subsets of runs in this table.

Stability of Integration Scheme—drift in Hamiltonian

For a stable integration scheme, we expect to see conservation of the total energy in the microcanonical ensemble to a reasonable degree. We qualify the use of "reasonable", noting that the use of a short-range cutoff for non-bonded interactions creates small fluctuations in total energy as particles move across the cutoff threshold. We attempted to detect systematic drift in energy and temperature by computing sub-block averages over subsets of the total trajectory. For most short (2 ns) runs no definitive drift could be observed. Longer runs using the MTS integrator with $\delta t_{\text{outer}} \leq 6$ fs (runs 16–18), or the Verlet integrator with $\delta t \leq 5$ fs (runs 1–5), exhibited no observable drift in energy and temperature. Obvious pathology was observed in run 12, with the large timestep for non-bonded and 3–4 intramolecular interactions of 8 fs. Different combinations of multiple timesteps with an outer timestep of 8 fs (runs 13–15) markedly improve the apparent stability of the integrator. Long runs of 30 ns were required to accurately gauge the drift rates of energy and temperature. Figure 1 depicts the energy drift rates for runs 13–15, which are estimated by linear fits to the energy subblock profiles obtained over the course of the simulations. The drift rates in the Hamiltonian, dE^*/dt, for these runs are estimated at $1.5 \times 10^{-6} \pm 1.5 \times 10^{-7}$, $1.2 \times 10^{-6} \pm 1.1 \times 10^{-7}$, and $2.5 \times 10^{-6} \pm 6.2 \times 10^{-8}$ ps^{-1}, respectively. The corresponding effect on temperature is less pronounced and is shown in Fig. 2. Similar estimates on the temperature drift, dT/dt, yields rates of 0.04 ± 0.01, 0.02 ± 0.01, and 0.07 ± 0.01 K/ns, respectively. Dysthe *et al.* [3] suggested that as long as a trajectory does not exceed the (drift-subtracted) variance in temperature, measured quantities along the trajectory should not be unduly affected. In the present case, the variance in subblock averaged temperature is approximately 5.5 K, suggesting that this limit would be exceeded after 128, 230, and 74 ns for runs 13, 14, and 15, respectively. While these numbers are only approximate due to the uncertainties associated with the computed drift rates, it does give us an estimate of the limits of such an integration scheme. We also note that Dysthe *et al*. [3] report similar temperature drift rates, but of opposite sign (-0.02 to -0.08 K/ns) on liquid *n*-decane systems using the velocity Verlet-based RATTLE algorithm [10] for integration of the equations of motion subject to the constraints of fixed bond lengths.

Atomic and Molecular Pressure

The elements of the pressure tensor can be described in both atomic and molecular formalisms, and both have been employed in the evaluation of

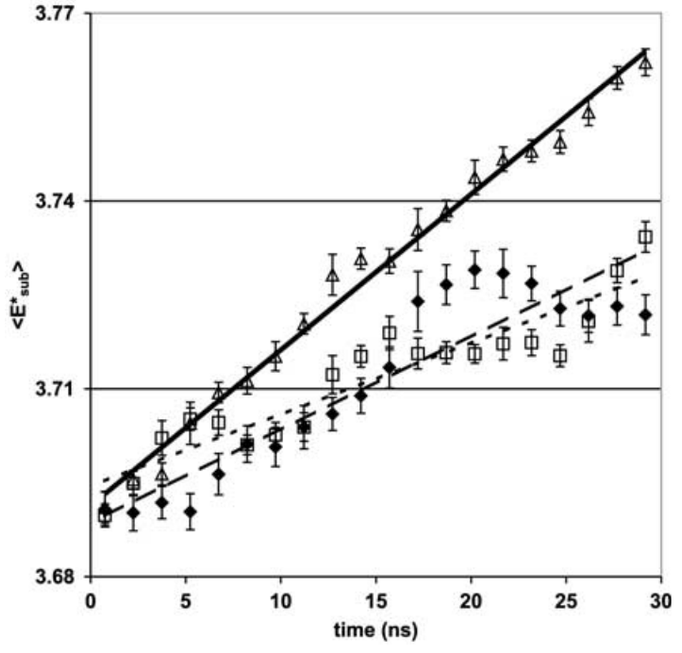

FIGURE 1 Drift plots of total energy during 30 ns NVE dynamics of liquid *n*-octane system. Different runs correspond to multiple timestep factorizations outlined in Table I with an outer timestep of 8 fs. Δ; run 17, □; run 18, ◆; run 19. These parameters reside close to the edge of the integrator stability for microcanonical dynamics.

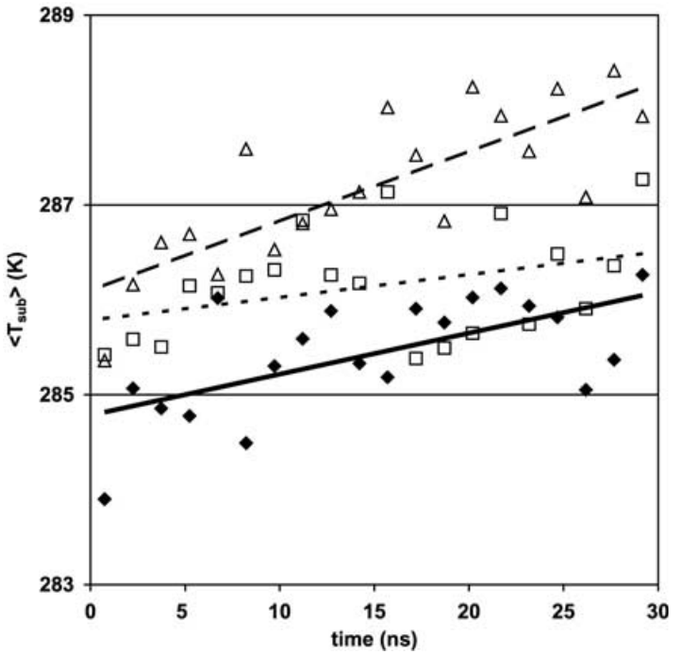

FIGURE 2 Drift plots of temperature during 30 ns NVE dynamics of liquid *n*-octane system. Runs and symbols are the same as Fig. 1.

the pressure tensor. In the atomic formalism this can be written as [11]

$$P_{\alpha\beta}^{\text{atom}} = \frac{1}{V}\left[\sum_{i,a}^{\text{atoms}} m_i (v_{ia})_\alpha (v_{ia})_\beta + \sum_{i,a}\sum_{\substack{j,b \\ i\neq j}} (\vec{r}_{ia} - \vec{r}_{jb})_\alpha (f_{ia-jb})_\beta + \sum_{i,a} (\vec{r}_{ia} - \vec{r}_{i,\text{com}})_\alpha (f_{ia}^{\text{intra}})_\beta\right] \quad (1)$$

where the subscript *ia* denotes atom *a* on molecule *i*, com refers to the center of mass, f_{ia-jb} is the force acting between atoms *a* and *b* on molecules *i* and *j*, and f_{ia}^{intra} denotes intramolecular forces on atom *a* of molecule *i*.

The molecular form of the pressure tensor employs center-of-mass positions, velocities and masses, and sums over only the *inter*molecular forces

$$P_{\alpha\beta}^{\text{molec}} = \frac{1}{V}\left[\sum_{i}^{\text{molecules}} m_{i,\text{com}} (v_{i,\text{com}})_\alpha (v_{i,\text{com}})_\beta + \sum_{i>j}^{\text{molecules}} (\vec{r}_{i,\text{com}} - \vec{r}_{j,\text{com}})_\alpha \sum_a \sum_b (f_{ia-jb})_\beta\right] \quad (2)$$

Equations (1) and (2) are not formally equivalent. Allen [12] showed that the atomic and the symmetrized molecular stress tensors are related (to first order) through a mass weighted orientation tensor as

$$\mathbf{P}^{\text{atomic}} = \mathbf{P}_{\text{sym}}^{\text{molec}} + \frac{1}{2}\ddot{\boldsymbol{\theta}} \quad (3)$$

where

$$\boldsymbol{\theta} = \sum_{i}^{\text{molecules}} \sum_{a}^{\text{atoms}} m_{i,a} \delta\vec{r}_{i,a} \delta\vec{r}_{i,a} \quad (4)$$

where $\delta\vec{x}_i = \vec{x}_i - \vec{x}_{i,\text{com}}$ are the atomic positions and velocities relative to the molecule's center of mass. The second time derivative can be expressed as

$$\ddot{\boldsymbol{\theta}} = \sum_i \left[2\sum_a m_{i,a} \delta\vec{v}_{i,a} \delta\vec{v}_{i,a} + \sum_a \delta\vec{r}_{i,a} \vec{f}_{i,a} + \sum_a \vec{f}_{i,a} \delta\vec{r}_{i,a}\right]. \quad (5)$$

In either formalism, the pressure is computed as the average over the diagonal elements of the appropriate tensor. Sensitivity of the atomic and molecular pressure to the size of integration timestep is evident in Fig. 3, which displays the computed pressure for runs 1–5 (velocity Verlet integration with $\delta t = 1$–5 fs) as a function of timestep. With a finely resolved timestep of 1 fs, the atomic and molecular pressures coincide. The average values of the diagonal elements of Eq. (5) were found to be very close to zero, as expected. As the timestep increases, the computed pressures deviate in opposite directions; the molecular pressure shows

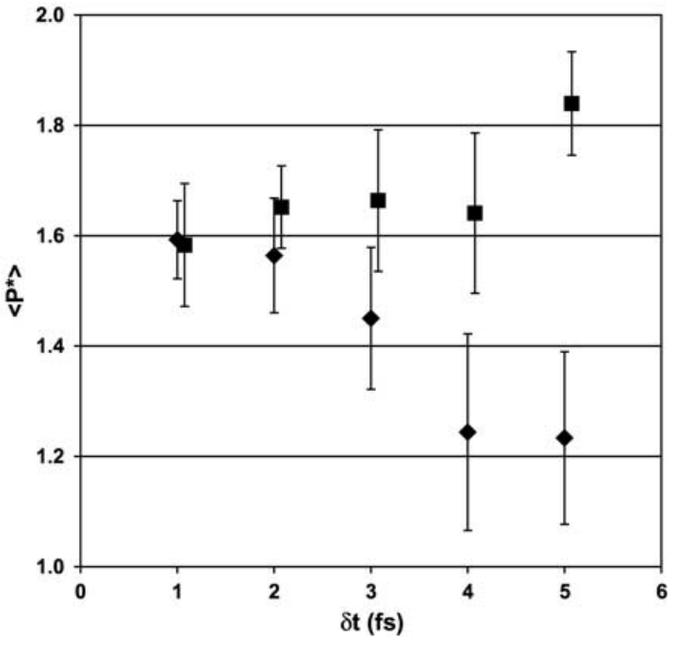

FIGURE 3 Atomic (◆) and molecular (■) pressure as a function of integration step size for velocity Verlet integration scheme for liquid *n*-octane system.

a modest increase and the atomic pressure shows a more drastic decline. In Fig. 4, several runs employing a multiple timestep scheme (runs 7, 10, 15, and 17) exhibit similar behavior for the atomic pressure. The molecular pressure appears more robust, displaying no apparent dependence on the magnitude of the outer timestep up to the 8 fs limit considered here. In conjunction with the multiple timestep integrator, this appears to be a decided advantage in the use of the molecular formalism. The observation that use of the Verlet integrator displays no apparent problems in energy conservation for $\delta t \leq 5$ fs, but

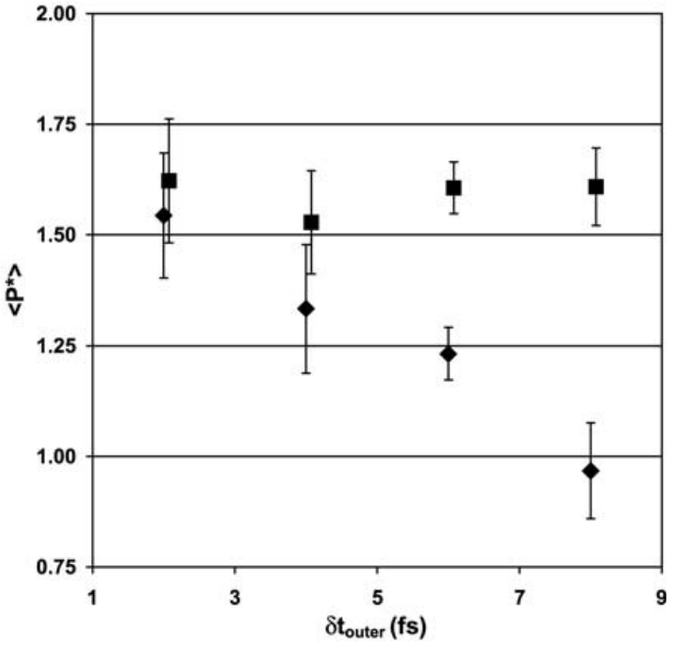

FIGURE 4 Atomic (◆) and molecular (■) pressure as a function of integration step size for the multiple timestep integrator. Multiple timestep integrator for runs 7 ($\delta t_{\text{outer}} = 2$ fs), 10*a* (4 fs), 21*a* (6 fs), and 18*a* (8 fs) are displayed.

shows obvious sensitivity to atomic and molecular pressure underscores the importance of stability checks for properties of interest to the specific application.

The findings of Mondello and Grest [13] on *n*-alkane systems appear to differ from our observations here. They employed a fixed-bond model, integrating the equations of motion with the RATTLE algorithm and timestep of 5 fs. They report that the atomic pressure is much less sensitive to details of the integration scheme employed. In addition, they note that, with a 5 fs timestep, molecular pressures were consistently 1–2 MPa higher than atomic pressures for systems of liquid *n*-alkanes. By contrast, we observe much greater sensitivity of the atomic pressure. Even multiple timestep schemes with short timesteps for bonded interactions do not appear to overcome this sensitivity, yet molecular pressures appear unaffected by the multiple timestep procedure.

These differences appear to stem from the fact that the RATTLE algorithm enforces zero force constraints on the bond lengths. This constraint will be satisfied to high precision independent of the size of the timestep. With our integration scheme and flexible bonds, inaccuracies associated with integrating the fast modes of the bonds appears to be the primarily source of error.

Atomic and Molecular Viscosity

Transport coefficients have been computed using the Green–Kubo formalism, which relates a macroscopic transport coefficient to the magnitude and decay of spontaneous fluctuations of a corresponding microscopic quantity. For example, the zero-shear viscosity is related to fluctuations in the off-diagonal elements of the stress (pressure) tensor

$$\eta = \frac{V}{kT}\int_0^\infty \left\langle P^{\mathrm{s}}{}_{\alpha\beta}(0) P^{\mathrm{s}}{}_{\alpha\beta}(t)\right\rangle \mathrm{d}t \tag{6}$$

where $P^{\mathrm{s}}_{\alpha\beta}$ is the instantaneous value of the stress tensor element $\alpha\beta$, V is the system volume, and T is the temperature. Averaging over the three independent off-diagonal stress tensor elements improves the convergence of Eq. (6). It has also been reported that improved statistics can be obtained by employing the six independent quantities in the symmetrized-traceless form of the pressure tensor [13,14]. The corresponding viscosity is computed as

$$\eta_{\mathrm{st}} = \frac{V}{10kT}\int_0^\infty \left\langle \sum_{\alpha\beta} P^{\mathrm{st}}_{\alpha\beta}(0) P^{\mathrm{st}}_{\alpha\beta}(t)\right\rangle \mathrm{d}t \tag{7}$$

with

$$\begin{aligned} P^{\mathrm{st}}_{\alpha\beta} &= P^{\mathrm{s}}_{\alpha\beta} - \delta_{\alpha\beta}\sum_\gamma P_{\gamma\gamma} \\ &= \frac{P_{\alpha\beta}+P_{\beta\alpha}}{2} - \delta_{\alpha\beta}\sum_\gamma P_{\gamma\gamma} \end{aligned} \tag{8}$$

The elements of the pressure tensor can be formulated in both atomic and molecular formalisms, as shown in Eqs. (1) and (2). It should be noted that the atomic pressure tensor is symmetric, but in general, the molecular analogue is not. A symmetrized form of the stress tensor is then used in the molecular formalism when applied to the Eq. (8).

In terms of Eq. (5), the relationship between the atomic and molecular stress-tensor autocorrelation function is

$$\begin{aligned} \left\langle P^{\mathrm{atom}}_{\alpha\beta}(t) P^{\mathrm{atom}}_{\alpha\beta}(0)\right\rangle &= \left\langle P^{\mathrm{molec}}_{\mathrm{sym},\alpha\beta}(t) P^{\mathrm{molec}}_{\mathrm{sym},\alpha\beta}(0)\right\rangle \\ &\quad + \left\langle \ddot{\theta}_{\alpha\beta}(t) P^{\mathrm{molec}}_{\mathrm{sym},\alpha\beta}(0)\right\rangle \\ &\quad + \frac{1}{4}\left\langle \ddot{\theta}_{\alpha\beta}(t)\ddot{\theta}_{\alpha\beta}(0)\right\rangle \end{aligned} \tag{9}$$

It has been generally assumed that the stress-tensor formalism employed in the calculation of the stress autocorrelation function yields essentially the same result when computing the viscosity. This has been verified numerically by several authors [11,15,16] for *n*-butane and *n*-decane case studies. The molecules were examined under conditions where the rotational relaxation times were short (e.g. *n*-decane at $T = 480\,\mathrm{K}$, $\rho = 0.6136\,\mathrm{g/cm^3}$ Cui *et al.* obtained $\tau_{\mathrm{rot}} = 10.2\,\mathrm{ps}$. We have also verified that the last two terms of Eq. (9) decay to zero on very short time scales even for systems with a somewhat longer orientational relaxation time. Figure 5(a) and (b) shows the autocorrelation functions of the last two terms of Eq. (9) for a 120 molecule liquid *n*-dodecane system at $T = 373\,\mathrm{K}$ and $\rho = 0.7034\,\mathrm{g/cm^3}$. A 15.5 ns trajectory was generated for liquid *n*-dodecane employing a velocity Verlet integrator with $\delta t = 1.25\,\mathrm{fs}$. Stress-tensor data was saved every timestep. This state point has a somewhat longer rotational relaxation time than those mentioned above ($\tau_{\mathrm{rot}} = 31\,\mathrm{ps}$), yet the decay of the autocorrelation functions is still quite rapid. The cumulative integration of these terms (with appropriate prefactor included from Eq. (7)) is also plotted and is seen to be a negligible contribution to viscosity, decaying to nearly zero within approximately 2 ps. Thus, we expect equivalent results for viscosity determined from the atomic and molecular formalism.

Returning to our *n*-octane example, cumulative integrals of Eq. (7) using the velocity Verlet integrator

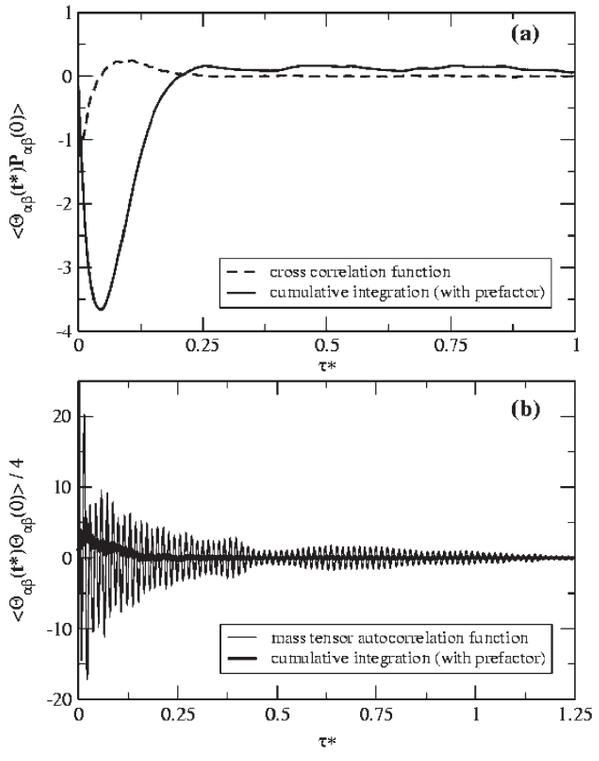

FIGURE 5 Relationship between atomic and molecular stress tensor formalisms for *n*-dodecane at $T = 373\,\mathrm{K}$. (a) Short time behavior of cross correlation function. (b) Short time behavior of autocorrelation function of second derivative of mass tensor. In both cases, the cumulative integral of the correlation function is shown, including the prefactor $V^*/\langle T^* \rangle$, as described in Eq. (7).

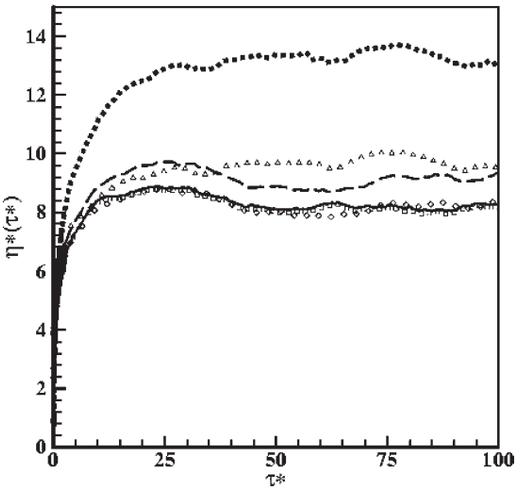

FIGURE 6 Cumulative viscosity curves for liquid *n*-octane at 293 K using atomic (lines) and molecular (points) stress tensor formalism and the velocity Verlet integrator. For atomic stress tensor data, (—) $\delta t = 1\,\mathrm{fs}$, (--) $\delta t = 3\,\mathrm{fs}$, (···) $\delta t = 5\,\mathrm{fs}$. For molecular stress tensor, (□) $\delta t = 1\,\mathrm{fs}$, (◇) $\delta t = 3\,\mathrm{fs}$, (Δ) $\delta t = 5\,\mathrm{fs}$.

are shown in Fig. 6. All runs in the figure were 10 ns in duration. We find excellent agreement between atomic and molecular formulae, with a timestep of 1 fs. As the timestep increases, the magnitude of the discrepancy between the atomic and molecular viscosity increases, with the atomic formula showing greater sensitivity to timestep. At $\delta t = 5\,\mathrm{fs}$, the plateau region of the atomic viscosity curve is over 50% greater than that obtained at $\delta t = 1\,\mathrm{fs}$. The molecular viscosity shows a modest increase in the plateau value of the curves, but not to the same extent as the atomic curves. These findings are consistent with the observations of the bulk pressure in the previous section.

We also noted that in cases where the equations of motion were integrated with a small timestep, the atomic-based viscosity is more sensitive to the frequency with which stress tensor data is employed in the evaluation of Eq. (7). Figure 7(a) and (b) shows the viscosity computed using the atomic and molecular formalism for the *n*-dodecane system of Fig. 5 using the same integrator and timestep, but now using stress tensor data sampled over larger time intervals. Even though the integration timestep is still highly refined, the atomic formalism shows more sensitivity to the larger spacing of saved data, becoming very inaccurate above a data spacing of approximately 20 fs.

Figure 8 shows the effect of increasing the outer timestep of the multiple timestep approach, keeping δt_{bond} and $\delta t_{3-4\,\mathrm{intra}}$ at 1.0 and 2.0 fs, respectively (runs 10, 14, 17, and 19). The observations are analogous to the bulk pressure; the atomic formula still exhibits an increase in the apparent plateau value with increasing timestep, while the molecular formalism appears to be somewhat more robust. We note that at this state point, the orientation relaxation time, τ_{ort}, of the molecules was found to be approximately 20 ps, meaning that the 10 ns trajectory over which the stress tensor was sampled for the autocorrelation function represents nearly 500 times this characteristic relaxation time.

The orientation relaxation time is often employed to determining a plateau region in the cumulative viscosity curve. In liquid *n*-alkanes systems, this characteristic time has been seen as the longest relaxation time of the system, and it is on this timescale that the stress autocorrelation function decays. We have chosen to fit the region $2\tau_{\mathrm{ort}} - 4\tau_{\mathrm{ort}}$ of the cumulative viscosity curves to determine the viscosity; these values are shown in Table II. Uncertainties were estimated applying the same procedure to 3 subblocks of the trajectory. The variance obtained for most multiple timestep runs in this way is on the order of 10%, while the single timestep runs have appreciable larger (12–18%) uncertainties. By way of comparison, based on their statistical analyses of long runs of *n*-hexadecane, Mondello *et al.* [13] determined that trajectories of

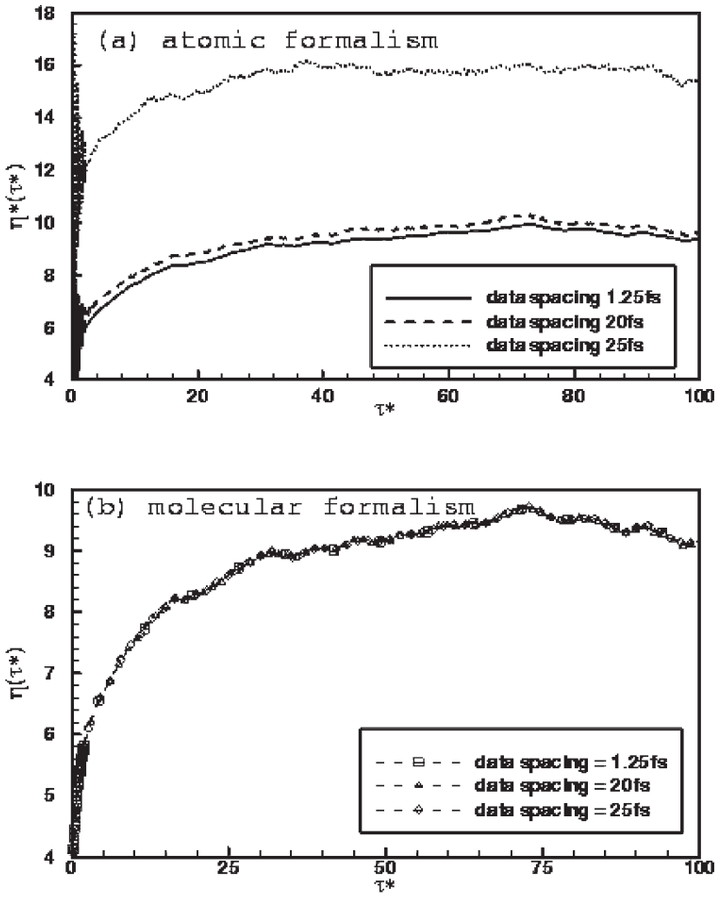

FIGURE 7 Computation of cumulative viscosity of *n*-dodecane at $T = 373\,\mathrm{K}$ using (a) atomic and (b) molecular stress-tensor formalism, with data saved with varying frequency. The equations of motion were integrated with a timestep of 1.25 fs and data was collected over a 15.5 ns trajectory.

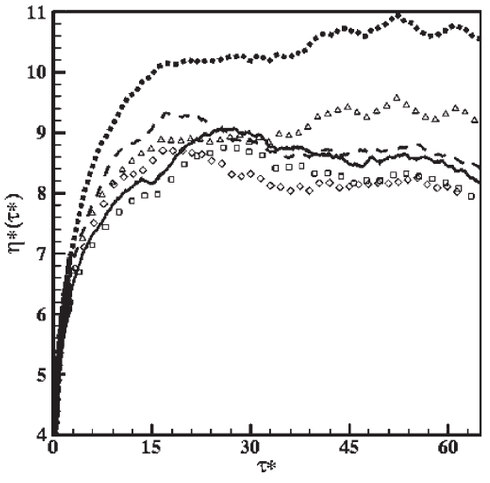

FIGURE 8 Cumulative viscosity curves for liquid *n*-octane at 293 K using atomic (lines) and molecular (points) stress tensor formalism and the multiple timestep integrator. For all multiple timestep factorizations $\delta t_{\mathrm{bond}} = 1\,\mathrm{fs}$, $\delta t_{3-4\,\mathrm{intra}} = 2\,\mathrm{fs}$, and each curve corresponds to different values of the outer timestep, $\delta t_{\mathrm{outer}}$. For atomic stress tensor data, (—) $\delta t_{\mathrm{outer}} = 2\,\mathrm{fs}$, (---) $\delta t_{\mathrm{outer}} = 4\,\mathrm{fs}$, $(\cdots)$ $\delta t_{\mathrm{outer}} = 6\,\mathrm{fs}$. For molecular stress tensor, (□) $\delta t_{\mathrm{outer}} = 2\,\mathrm{fs}$, (◇) $\delta t_{\mathrm{outer}} = 4\,\mathrm{fs}$, (△) $\delta t_{\mathrm{outer}} = 6\,\mathrm{fs}$.

duration 100–200 times the molecule rotational relaxation time should yield statistical uncertainties on the order of 10%.

The observed sensitivity of the atomic-based viscosity to the timestep appears consistent with the observations of Cui *et al.* [11] in the simulation of flexible bond models of liquid *n*-alkanes. In their comparison of atomic and molecular pressure tensor formalisms, they state that small timesteps are required to adequately capture the rapid oscillations present in the atomic stress tensor autocorrelation function. Again, we have not seen this effect reported in the literature with respect to fixed bond models. This is somewhat puzzling, since atomic viscosity must incorporate the constraint forces associated with the bonds. However, we assume that a constraint-based integrator such as RATTLE must resolve these forces fairly accurately for this not to be an issue. Errors associated with this integrator must propagate in a different way, although a detailed analysis of this effect is beyond the scope of our current work.

TABLE II Effect of integration timestep details on plateau values of atomic and molecular viscosity, and molecular diffusion derived from autocorrelation functions. Viscosity was determined from 10 ns NVE simulations, and diffusion from 4 ns trajectories.

					Atomic		*Molecular*		*Diffusion*	
Run	$\delta t_{(outer)}$ *(fs)*	$\delta t_{(bond)}$ *(fs)*	$\delta t_{(3-4\,intra)}$ *(fs)*	$\delta t_{(LJ)}$ *(fs)*	η_{GK} *(cP)*	$\pm\ \sigma$ *(cP)*	η_{GK} *(cP)*	$\pm\ \sigma$ *(cP)*	$D_{VACF} \times 10^5$ cm^2/s	$\pm\ \sigma \times 10^5$ cm^2/s
1	1.0				0.35	0.07	0.35	0.07	2.78	0.04
3	3.0	No multiple timestep employed			0.38	0.05	0.35	0.04	2.78	0.06
5	5.0				0.54	0.08	0.38	0.05	2.82	0.09
10	4.0	1.0	2.0	4.0	0.36	0.02	0.34	0.02	2.82	0.03
14	8.0	1.0	2.0	8.0	0.44	0.03	0.34	0.03	2.82	0.08
17	6.0	1.0	2.0	6.0	0.43	0.04	0.38	0.04	2.80	0.07
19	2.0	1.0	2.0	2.0	0.36	0.03	0.36	0.03	2.74	0.04

For comparison, we have also examined the self-diffusion coefficient computed from molecular center-of-mass displacement and the velocity autocorrelation function for the integrators listed in Table II. In contrast to the viscosity, the diffusion coefficients obtained showed little observable sensitivity to the size or factorization of the multiple timestep approach. In light of our previous observations, analysis of the sensitivity of the self-diffusion coefficient to simulation details would not give a complete picture of the relationship between the integrator and its influence on resulting properties.

CONCLUSIONS

The purpose of this note is to summarize our observations relating to the influence of simulation details on computed thermodynamic and transport properties relevant to fully flexible potentials employed as model lubricant components. Multiple timestep approaches with outer timesteps of up to 6 fs showed no obvious drift in energy or temperature over runs as long as 30 ns, runtimes commensurate with liquid paraffins in the C_8–C_{16} carbon number range. An outer timestep of 8 fs represents a rough upper limit on the stability of the integration schemes employed; measurable drift in energy and temperature were observed over tens of nanosecond trajectories.

We have found that the molecular-based description of the stress tensor is far less sensitive than the atomic formalism to details of the integration method and size of timestep employed. In addition, molecular-based quantities, including bulk pressure and transport coefficients such as viscosity and diffusion appear stable (within the statistical uncertainties of the computations) with respect to the multiple timestep factorization with $\delta t_{\text{outer}} \leq 8$ fs. For the flexible hydrocarbon models of interest in this work, the use of a multiple timestep integrator with a 6 fs outer timestep (such as runs 16–18 in Table I) gives reasonable speedup of the computation, while maintaining stability of the integration scheme.

References

[1] Allen, M.P. and Tildesley, D.J. (1987) *Computer Simulation of Liquids* (Clarendon Press, Oxford).
[2] Haile, J.M. (1992) *Molecular Dynamics Simulation* (John Wiley & Sons, New York).
[3] Dysthe, D.K., Fuchs, A.H. and Rousseau, B. (1999) "Fluid transport properties by equilibrium molecular dynamics. I. Methodlogy at extreme fluid states", *J. Chem. Phys.* **110**, 4047.
[4] Gordon, P.A. (2003) "Modeling structure property relationships in synthetic basestocks", In: Braihman, Y., eds, *Dynamics and Friction at Sub-Micron Confining Systems* (American Chemical Society, In press.
[5] Martin, M.G. and Siepmann, J.I. (1999) "Novel configurational-bias Monte Carlo method for branched molecules. Transferable potentials for phase equilibria. 2. United-atom description of branched alkanes", *J. Phys. Chem. B* **103**, 4508.
[6] Jorgensen, W.L., Madura, J.D. and Swenson, C.J. (1984) "Optimized intermolecular potential functions for liquid hydrocarbons", *J. Am. Chem. Soc.* **106**, 6638.
[7] Plimpton, S.J., Pollack, E.L., Stevens, M.J., Simon, E.J., Carpenter, J.E., Lustig, S.R., Belak, J. and Stouch, T.R. (1999) Large Atomic and Molecular Massively Parallel Simulator (LAMMPS).
[8] Tuckerman, M., Berne, B.J. and Martyna, G.J. (1992) "Reversible multiple time scale molecular dynamics", *J. Chem. Phys.* **97**, 1990.
[9] Sergi, A., Ferrario, M. and Costa, D. (1999) "Reversible integrators for basic extended system molecular dynamics", *Mol. Phys.* **97**, 825.
[10] Andersen, H.C. (1983) "Rattle: a "velocity" version of the shake algorithm for molecular dynamics calculations", *J. Comput. Phys.* **52**, 24.
[11] Cui, S.T., Cummings, P.T. and Cochran, H.D. (1996) "The calculation of the viscosity from the autocorrelation function using molecular and atomic stress tensors", *Mol. Phys.* **88**, 1657.
[12] Allen, M.P. (1984) "Atomic and molecular representations of molecular hydrodynamic variables", *Mol. Phys.* **52**, 705.
[13] Mondello, M. and Grest, G.S. (1997) "Viscosity calculations of *n*-alkanes by equilibrium molecular dynamics", *J. Chem. Phys.* **106**, 9327.
[14] Daivis, P.J. and Evans, D.J. (1993) "Comparison of constant pressure and constant volume nonequilibrium simulations of sheared model decane", *J. Chem. Phys.* **100**, 541.
[15] Cui, S.T., Cummings, P.T. and Cochran, H.D. (1996) "Multiple time step nonequilibrium molecular dynamics simulation of the rheological properties of liquid *n*-decane", *J. Chem. Phys.* **104**, 255.
[16] Marechal, G. and Ryckaert, J.P. (1983) "Atomic versus molecular description of transport properties in polyatomic fluids: *n*-butane as an illustration", *Chem. Phys. Lett.* **101**, 548.